

## A Woodpecker' s Tongue-Inspired, Bendable and Extendable Robot Manipulator With Structural Stiffness

Matsuda, Ryota

Faculty of Mechanical Engineering, Kyushu University

Mavinkurve, Ujjal Krishnan

Faculty of Mechanical Engineering, Kyushu University

Kanada, Ayato

Faculty of Mechanical Engineering, Kyushu University

Honda, Koki

Faculty of Mechanical Engineering, Kyushu University

他

<https://hdl.handle.net/2324/7172242>

---

出版情報 : IEEE Robotics and Automation Letters. 7 (2), pp.3334-3341, 2022-01-31. Institute of Electrical Electronics Engineers (IEEE)

バージョン :

権利関係 : © 2022 IEEE. Personal use of this material is permitted. Permission from IEEE must be obtained for all other uses, in any current or future media, including reprinting/republishing this material for advertising or promotional purposes, creating new collective works, for resale or redistribution to servers or lists, or reuse of any copyrighted component of this work in other works.





# A Woodpecker's Tongue-inspired, Bendable and Extendable Robot Manipulator with Structural Stiffness

Ryota Matsuda<sup>1</sup>, Ujjal Krishnanand Mavinkurve<sup>1</sup>, Ayato Kanada<sup>1</sup>, Koki Honda<sup>1</sup>,  
Yasutaka Nakashima<sup>1</sup>, and Motoji Yamamoto<sup>1</sup>

**Abstract**—Woodpeckers have flexible and extendable tongues that they use to reach their prey through tiny openings in trees and insect burrows. This unique capability of their tongue represents a promising design for a tool for picking up and handling objects in unstructured environments. Although continuum robots can produce dexterous movements because of their few shape constraints, the lack of structural stiffness has restricted their deployment in real-world environments. Inspired by the characteristics of woodpeckers, we designed a robot manipulator that can substantially extend its length and bend its shape in 2D space. This behavior is enabled by a backbone consisting of a chain of rigid joints and two flexible rack gears. The joints increase the payload by structurally supporting the robot. The proposed structure is 4.7 times stronger in vertical bending and 6.2 times stronger in torsion than without rigid links. Feeding the rack gears at the same and different speeds allows the robot to elongate and bend, respectively. We developed a geometric model based on a constant curvature model for motion planning. Experiments show that the robot can follow an arbitrary trajectory at an arbitrary tip angle. Lastly, we showcase various demonstrations, including deployment and storage for the backbone, follow-the-leader (FTL) motion, and whole-arm grasping in the horizontal plane.

**Index Terms**—Flexible robots, continuum robots, bio-inspired robots, Woodpeckers.

## I. INTRODUCTION

Extending and bending are effective ways to improve the workspace of end-effectors in both natural and artificial systems. For example, frogs, chameleons, and anteaters are animals that are well-known for their extendable and bendable tongues that they use to retrieve food from a distance [1]. A robotic manipulator with these capabilities would be advantageous. For example, this kind of manipulator would be able reach a product on the back of a cluttered shelf. Such a concept is promising for applications which require picking and handling actions in unstructured environments, but to-date

only exists in science fiction and fantasy (e.g., Doctor Octopus from Spider-Man [2]).

Continuum robots are those with manipulators that are inspired by the lightweight and flexible structures of animals [3]–[7]. Their high compliance and environmental adaptability are attractive for use outside of highly technical sites, wherein there are frequent risk of contacts with obstacles or people, necessitating a more flexible manipulator. Many continuum robots are capable of only bending motion, but some are capable of both extension and bending actions. For example, soft continuum manipulators have a stretchable backbone, including springs, origami, and telescopic pipes to extend their lengths [8]–[12]. They can turn in any direction but at the cost of the extension distance due to design limitations of the elasticity of springs and origami or the diameter of telescopic pipes. Plant root-inspired robots achieve growth from the tip by pressurizing flexible, thin-walled tubes, with a length change of hundreds to thousands of percent [13]–[15]. However, they require additional actuators to perform the repetitive bending motion and also tend to bend or buckle into an uncontrollable shape when retracted. These extendable soft mechanisms lack structural stiffness, making it challenging to use them in many applications, particularly those which require the grabbing and carrying of objects. Although continuum robots with rigid elements in the backbone have been studied [16], [17], they are not stretchable. In contrast, extendable rigid mechanisms, including pantographs [18], telescopic cylinders [19], and self-locking joints [20], have high payloads, but are restricted in their bending motions due to their stiffness. Attempts have been made to build an origami-inspired extendable robot that consists entirely of rigid parts to overcome bending limitations [21]. These rigid structures can result in unsafe interactions with humans and objects if they apply too much force.

This paper argues that a combination of soft and rigid components is necessary to achieve both high stiffness and actuation of extending and bending. We focused on woodpeckers with excellent tongue manipulators, consisting of a linear series of tiny bones (called hyoid bones) sheathed in muscles and soft tissue [22], [23]. The extremely long tongue can bend and extend to reach insects through small openings and raised burrow systems (Fig. 1). We focus on the following four functions of the woodpecker:

- A hyoid apparatus. Unlike the human and anteater tongues, which are made mainly of muscle, the woodpecker's tongue is rigidly supported by the hyoid bones,

Manuscript received: October 16, 2021; Revised: December 26, 2021; Accepted: January 18, 2022.

This paper was recommended for publication by Editor Cecilia Laschi upon evaluation of the Associate Editor and Reviewers' comments. This work was supported in part by the Grant-in-Aid for Research Activity Start-up under Grant 20K22398 and Innovation inspired by Nature" Research Support Program, SEKISUI CHEMICAL CO., LTD. (Corresponding author: Ayato Kanada)

<sup>1</sup>R. Matsuda, U. K. Mavinkurve, A. Kanada, K. Honda, Y. Nakashima, and M. Yamamoto are with Faculty of Mechanical Engineering, Kyushu University, 819-0395 Fukuoka, Japan.  
kanada.ayato.853@m.kyushu-u.ac.jp

Digital Object Identifier (DOI): see top of this page.

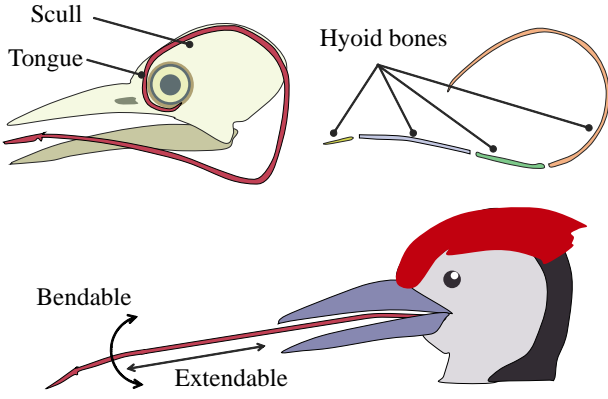


Fig. 1: Lateral view of the skull, hyoid bones, and head of woodpeckers. The long tongue, consisting of muscles and hyoid bones, can wrap itself around the head for storage and extend and bend in any direction.

extending straight out against gravity.

- A folding mechanism. The woodpecker's long tongue passes under the base of the jaw and wraps around the back and top of the head to fold it into the small head.
- A bending mechanism. Paired with intrinsic muscles covering the hyoid bones, it can control the bending movement of the tongue.
- An extending mechanism. The hyoid bones are not directly connected to the skull; hence the tongue can slide straight over a wide area, resulting in an highly extensible mechanism.

To reproduce these functions, we propose a manipulator that consists of soft and rigid components that is inspired by the woodpecker tongue, as shown in Fig. 2. A chain of rigid links resembling the hyoid bones is connected by revolute joints. It provides the flexibility to safely work in unstructured environments in the horizontal plane and the stiffness to handle heavy workloads in the vertical plane. Two flexible rack gears, which resemble the paired intrinsic muscles of the woodpecker tongue, pass through each link. Their front ends are fixed to the first link, and their back ends are free. The rear part of the manipulator, without the constraint of the fixed rack gears, is more flexible and easier to fold than the others, as shown in the upper part of Fig. 2. The two driving units can bend and elongate the manipulator in 2D space by moving the paired rack gears relative to themselves, as shown in the lower part of Fig. 2. In addition, the rigid chain is not directly fixed to the robot base, resulting in a long extension distance that depends on the length of the tongue. The remainder of this paper is organized as follows. In Section II, we describe a geometric model and a motion-planning method to control the robot manipulator. Section III presents the design and architecture of the proposed mechanism. Section IV shows the work-space, stiffness, maximum bending angle, trajectory tracking, and demonstration of the prototype. Finally, Section V concludes the article.

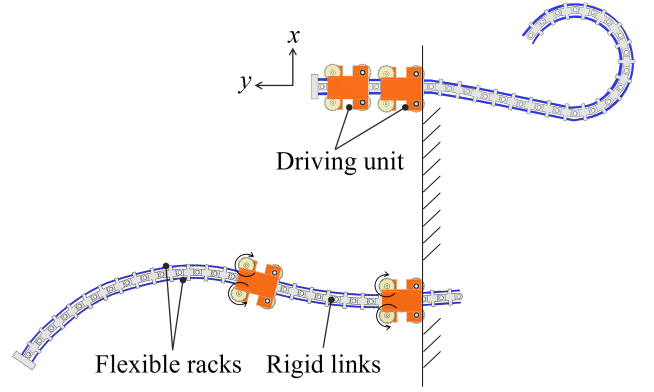


Fig. 2: Top view of the proposed robot manipulator. It consists of four degrees of freedom (DoF) systems, including two driving units with pinion gears and rigid links with two flexible rack gears. It is inspired by a woodpecker's tongue, and has a bendable and extendable body.

## II. DESIGN AND CONTROL

### A. Robot Design

The proposed robot consists of a chain of rigid links that acts as a backbone and two driving units that control the extension and bending of the body, as shown in Fig. 3(a). Each link was 3D printed with acrylonitrile butadiene styrene (ABS) plastic and was joined to each other by a rotary joint consisting of an oilless bushing and a screw on the yaw axis (Fig. 3(b)). The rigid links have sliders (grooves) on both sides to pass through the two flexible rack gears (molded flexible racks with a module of 0.8, KHK Co. Ltd.). The two rack gears are fixed at one end to the first joint and free at the other end, and their parallel distance was constrained to prevent buckling by the sliders. When either the left or right rack gear is pulled while the rear end link is fixed, the backbone is bent in an arc by the rack gears whose deformation is constrained. The flexibility of rack gears allows robots to work on horizontal surface compliance for safety. Two driving units pass inside the backbone: one is fixed to the robot base, and the other moves along the backbone. Four gears in the driving unit (two of which are passive and the two are connected to the motors) hold the backbone via the rack gears, as shown in Fig. 3(c). Rotating the gear attached to the motor (1000:1 Micro Metal Gearmotor HP 6V, Pololu Co.) moves the rack gear laterally relative to the driving unit. The backbone extends and bends by controlling the length of each rack gear relative to the driving units. The concept of the drive unit, which runs on the flexible gears that constitute the body of the manipulator, is based on our previous work [24], [25]. Table I lists some of the mechanical properties of the proposed robot.

### B. Kinematic Modeling

In this section, we define the kinematic model of the robotic manipulator and describe its forward and inverse kinematics. As explained in the previous section, the planar manipulator consists of two flexible racks driven by four pinions. This

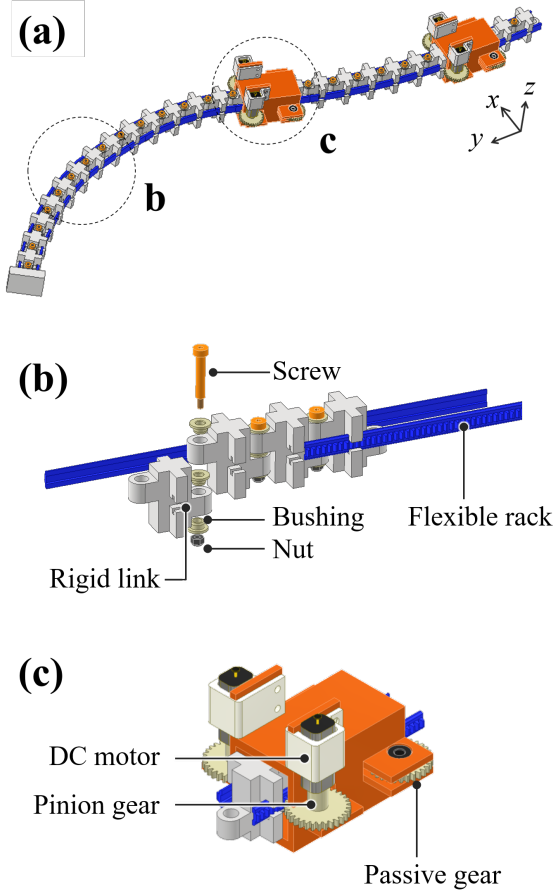


Fig. 3: Schematic diagram of the proposed mechanism. (a) Overview. (b) Backbone. (c) Driving unit.

design of the continuum robot allows us to change the lengths  $L = [L_1, L_2, L_3, L_4]$  by changing the pinion angles. These four rack lengths control the curvature  $[k_1, k_2]$  and the arc-length  $[S_1, S_2]$  shown in Fig. 4. to change the final position and orientation of the end-effector  $[x_F, y_F, \psi_F]$ . Since flexible rack gears can be regarded as thin beams, we apply the constant curvature approximation to the model. The homogeneous transformation can be obtained from Denavit–Hartenburg (D-H) parameters [26]. In our case, we consider each of the two driving units to be a Revolute-Prismatic-Revolute (RPR) manipulator. Hence, we can represent the continuum robot as the RPR-RPR manipulator. We convert the lengths of rack  $[L_1, L_2, L_3, L_4]$  to curvature and arc-length  $[k_1, k_2, S_1, S_2]$  as

TABLE I: The main specifications of the prototype manipulator

Robot Characteristics	Value
Backbone length (20 links)	500 mm
Payload	200 g
Minimum bending radius	30 mm
Robot mass	379 g
Circuit mass	92 g
Total mass	471 g

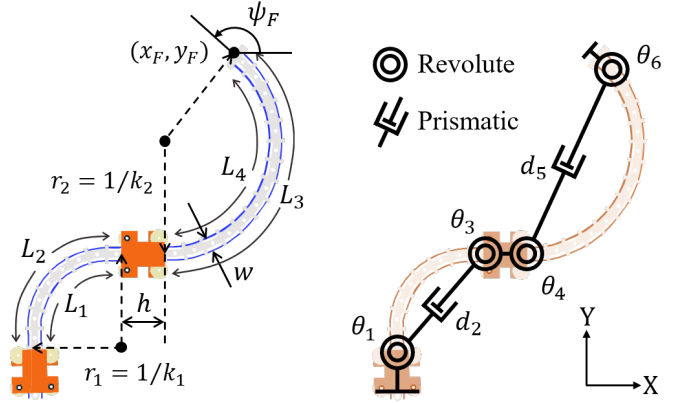


Fig. 4: Kinematic model of the proposed manipulator. We use an equivalent DH-type model with two RPR manipulators in series.

follows:

$$k_1 = \left( \frac{L_2 - L_1}{L_2 + L_1} \right) \frac{2}{w}, \quad k_2 = \left( \frac{L_4 - L_3}{L_3 + L_4} \right) \frac{2}{w}$$

$$S_1 = \frac{L_1 + L_2}{2}, \quad S_2 = \frac{L_3 + L_4}{2} \quad (1)$$

where  $w$  denotes the width between the rack gears. The sign of  $[k_1, k_2]$  determines the direction of turning of the manipulator with positive as a clockwise direction of turning. We convert these co-ordinates to the equivalent D-H parameters with  $[\theta_1, d_2, \theta_3]$  being the parameters for the first drive unit and  $[\theta_4, d_5, \theta_6]$  being the parameters for the second drive unit. The conversion from the continuum manipulators parameter  $[k_1, k_2, S_1, S_2]$  to D-H parameters  $[\theta_1, d_2, \theta_3, \theta_4, d_5, \theta_6]$  is as follows:

$$\begin{bmatrix} \theta_1 \\ d_2 \\ \theta_3 \\ \theta_4 \\ d_5 \\ \theta_6 \end{bmatrix} = \begin{bmatrix} \frac{\pi - k_1 S_1}{2} \\ \left| \frac{2}{k_1} \sin \left( \frac{k_1 S_1}{2} \right) \right| \\ -\frac{k_1 S_1}{2} \\ -\frac{k_2 S_2}{2} \\ \left| \frac{2}{k_2} \sin \left( \frac{k_2 S_2}{2} \right) \right| \\ -\frac{k_2 S_2}{2} \end{bmatrix} \quad (2)$$

We further compute the transformation matrix for each of the RPR manipulators  ${}^0T_4$  for the first and  ${}^4T_6$  for the second manipulator. The first transformation matrix  ${}^0T_4$  contains the offset introduced by the second driving unit. The transformation matrices of each of the RPR manipulators as well as the final transformation matrix  ${}^0T_6$  are as follows :

$${}^0T_4 = \begin{bmatrix} c(\theta_1 + \theta_3) & -s(\theta_1 + \theta_3) & 0 & d_2 c(\theta_1) + h c(\theta_1 + \theta_3) \\ s(\theta_1 + \theta_3) & c(\theta_1 + \theta_3) & 0 & d_2 s(\theta_1) + h s(\theta_1 + \theta_3) \\ 0 & 0 & 1 & 0 \\ 0 & 0 & 0 & 1 \end{bmatrix}$$

$${}^4T_6 = \begin{bmatrix} c(\theta_4 + \theta_6) & -s(\theta_4 + \theta_6) & 0 & d_5 c(\theta_4) \\ s(\theta_4 + \theta_6) & c(\theta_4 + \theta_6) & 0 & d_5 s(\theta_4) \\ 0 & 0 & 1 & 0 \\ 0 & 0 & 0 & 1 \end{bmatrix}$$

$${}^0T_6 = {}^0T_4 {}^4T_6 \quad (3)$$

where  $s$  and  $c$  denote sine and cosine function, respectively, and  $h$  shows the height of the driving unit. In the above equations, there is a singularity when the manipulator is straight. To overcome this problem, we maintain a minor difference in rack lengths  $[L_1, L_2]$  and  $[L_3, L_4]$ . Although forward kinematics of the manipulator can be obtained from Eq. 3, the inverse kinematics cannot be determined analytically as a unique solution because of a redundant degrees of freedom. To obtain the inverse kinematic solution, we used a nonlinear constraint-based optimization, which will be discussed in more detail in the next section.

### C. Motion Planning

We present the optimization-based motion planning approach used to solve the inverse kinematics of the manipulator. Given the endpoint and desired orientation of the end-effector  $X_{des} = [x_F, y_F, \psi_F]$ , we compute the input rack lengths  $L$  subject to certain constraints of the manipulator. We achieved this using sequential least squares programming (SLSQP), a non-linear constraint-based optimization method. We define the cost function  $f(L)$  as follows:

$$f(L) = \left| \frac{L_1 + L_2}{2} - \frac{L_3 + L_4}{2} \right| \quad (4)$$

The algorithm is explained in Algorithm 1.  $L$  is the optimization variable,  $[L_{prev}, L_{opt}, X_{opt}]$  are variables computed during optimization and  $[X_{des}, L_{max}, k_{max}]$  is the required data for optimization.  $L_{prev}$  contains the rack lengths of previous instance while  $L_{opt}$  and  $X_{opt}$  are the optimized rack lengths and end-effector co-ordinates obtained from the SLSQP optimization algorithm. The continuum robot's maximum arc length and curvature are limited to  $L_{max}$  and  $k_{max}$ , respectively. From  $X_{des}$ , we initialize the arc lengths  $L$  of the manipulator. We calculate the cost function based on the optimized rack lengths  $L_{opt}$  and the previous instant rack lengths  $L_{prev}$  compute the cost function, shown in Eq. 4. We then compute  $[L_{opt}, X_{opt}]$  based on SLSQP optimization subject to four constraints. The first constraint ensures that the optimized end-effector coordinates  $X_{opt}$  are reaching the desired endpoint  $X_{des}$ . The second constraint ensures the sum of the rack lengths before and after the second driving unit are always less than or equal to the maximum possible extension of the rack  $L_{max}$ . The third constraint limits the maximum possible curvature  $[k_1, k_2]$  to  $k_{max}$ . Lastly, we limit the rack lengths to be strictly non-negative values. The optimization process is terminated when the difference between the subsequent values of the cost function becomes less than or equal to zero.

## III. EXPERIMENTS

### A. Workspace

A significant advantage of the proposed robot is its ability to change length by the rack and pinion mechanism, augmenting reachability. To highlight this advantage, we compare the workspace of our continuum robot with a conventional extensible continuum robot by using the kinematic model mentioned in section II-B. Our robot can vary all four rack

---

### Algorithm 1 SLSQP for inverse kinematics

---

**1. Parameters:**

2.  $X_{des} = [x_F, y_F, \psi_F]$

**3. Routine:**

4. *Initialize*  $L$

5. **while** ( $\Delta f(L) \geq 0$ )

$L_{opt}, X_{opt} = \text{optimize\_slsqp}(f(L), L_{prev})$

**Constraints :**

1.  $X_{opt} = X_{des}$

2.  $L_1 + L_3 \leq L_{max}, L_2 + L_4 \leq L_{max}$

3.  $k_1, k_2 < k_{max}$

4.  $L \geq 0$

$L_{prev} = L_{opt}$

6. **end while**

7. **Update**  $L$

---

lengths from zero to maximum rack length  $L_{max}$  while satisfying the four constraints mentioned in section II-C. On the other hand, the conventional continuum robot driven by wires has a limited extension and retraction restricted by the following two reasons. First, springs, which are often used as compressible backbones in continuum robots, can only be shrunk to about half their length. Second, the spring length does not increase since the robot bends and contracts by pulling wires. To reproduce these two characteristics in our model, we change the second constraint in section II-C to  $L_{max}/4 \leq [L_1, L_2, L_3, L_4] \leq L_{max}/2$ . We numerically visualized the endpoints for each of these robots using the parameters shown in Table II. As shown in Fig. 5, the proposed manipulator can reach points in the neighborhood near the origin and improve the workspace area by 30 percent compared to the conventional manipulator. This is because our mechanism can determine the section lengths in the range of zero to the robot length by moving the driving unit; in contrast, the conventional mechanism can only reduce the section lengths by half by pulling wires.

### B. Stiffness

We aimed to achieve both high payload and high flexibility of the robot manipulator by employing rigid links to only increase the stiffness in specific directions. To demonstrate this, we examined how the stiffness of the robot manipulator changed with the presence of rigid links. Without rigid links, the backbone consists of two flexible rack gears and a plastic part at the end. The three test directions were in the direction of gravity ( $z$ -axis), horizontal ( $x$ -axis), and roll ( $y$ -axis)

TABLE II: Parameters for Workspace Simulation

Robot Characteristics	Value
$L_{max}$	440 mm
$k_{max}$	$0.033 \text{ mm}^{-1}$
$w$	21 mm
$h$	60 mm

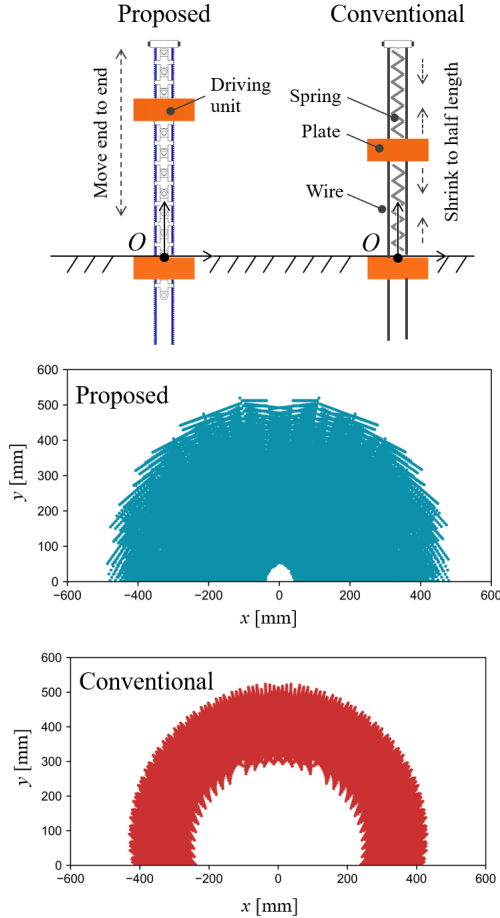


Fig. 5: Workspace comparison between proposed and conventional manipulator when changing arc length [ $L_1, L_2, L_3, L_4$ ].

reference), shown in the upper part of Fig. 6. Investigating torsion resistance is important because existing continuum robots are subjected to excessive torsion when subjected to offset loads, resulting in reduced dexterity and accuracy. A single driving unit with a backbone was fixed to the base, and the distance from one end of the backbone to the front surface of the driving unit was 50 mm. The stiffness was measured when the displacement or torsion was applied to the end of the manipulator by a force gauge (FGJN-5; NIDEC, Japan) attached to a digital ruler (SDV-45E; Mitutoyo, Japan). The stiffness was defined as the inclines of the force or torque-displacement curves that were obtained using the least-squares method. The error bars indicate the standard deviations of the five tests in the lower part of Fig. 6. In the  $z$ -axis and roll-axis directions, the stiffness was more than 4.7 and 6.2 times higher with the rigid link than without, respectively. Alternatively, in the  $x$ -axis direction, there was no significant difference in the stiffness between the cases with and without rigid links. This is due to a high stiffness of our rigid link in the  $z$ - and roll-directions coupled with a low stiffness in the  $x$ -direction.

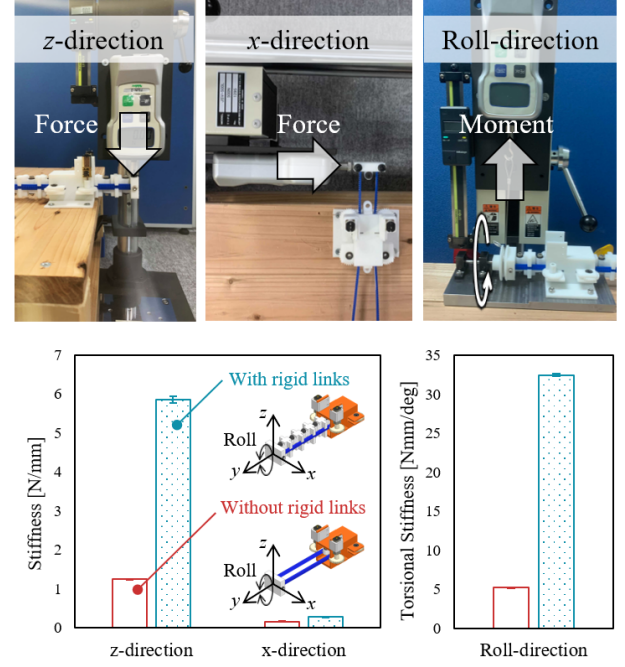


Fig. 6: Manipulator stiffness with and without the rigid links. The upper panel shows the experimental setup for measuring stiffness. The graph in the lower panel shows the stiffness in the  $x$ -axis,  $z$ -axis, and roll-axis for the three cases (error bars indicate SD from the five tests).

### C. Bending angle

The rigid links not only act as supports to increase stiffness, but also function as constraints to bend the manipulator into an arc. The upper panel of Fig. 7 shows the experimental setup used to investigate how the bending angle of the backbone changed with the presence of rigid links. A single driving unit with a backbone was fixed to the robot base. Initially, the lengths of both the left and right rack gears were set to 100 mm; that is, the backbone was straight. When the left rack gear is pulled, and the right rack gear is pushed, the backbone turns to the left. The bending angle with respect to the difference in the lengths of the left and right rack gears was measured using a motion tracker (OptiTrack V120; Trio; Acuity Inc., Japan). The lower panel of Fig. 7 compares the experimental results with and without rigid links, with the bending angles calculated from the constant curvature model. The error bars indicate the standard deviations of the five tests. The results with the rigid link follow the constant curvature model well, whereas the results without the rigid link do not follow the model as the bending angle increases. This is because one of the rack gear bulges outward so severely that the distance between the two rack gears is no longer constant, thus limiting the bending angle.

### D. Trajectory tracking

Our robot manipulator has two drive units (four DoFs in total) that feed the flexible rack gears back and forth, allowing the end-effector to reach any coordinate in planar space



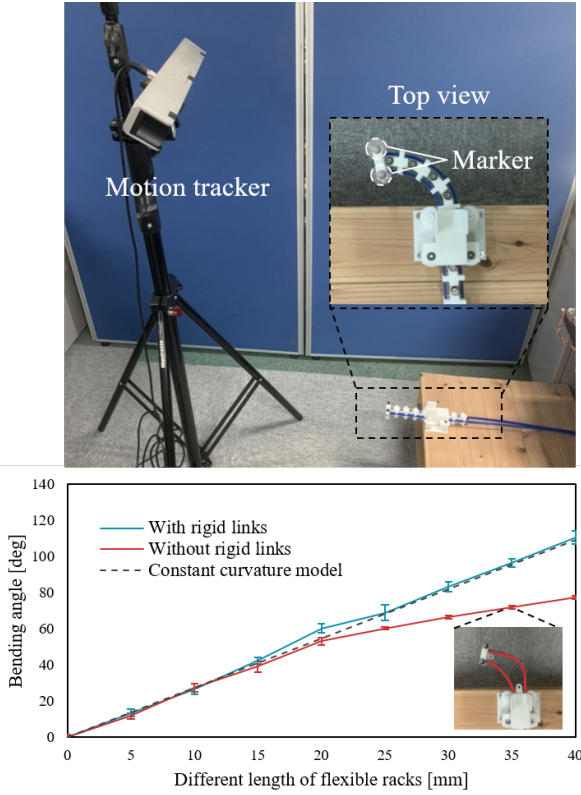


Fig. 7: Bending angle with and without the rigid links. The upper panel shows the experimental setup for measuring the bending angle. The graph in the lower panel shows the bending angle when changing the lengths of the two flexible rack gears (error bars indicate SD from five tests).

at any angle. For the demonstration of trajectory-following experiments, a sine curve with an amplitude of 50 mm and a wavelength of 400 mm was set at a distance of 200 mm from the end of the second driving unit fixed to the base. This curve was approximated by 40 points prepared from our motion planning. Target values for each motor were determined by linear interpolation of the point-to-point movement. While keeping the tip angle at 60 or 90 degrees, the end-effector is made to draw the same curve three times at a constant speed (20 s per lap) to evaluate repeatability. The experimental setup was the same as that in Fig. 8, and the motion tracker tracked a marker on the end-effector at a frame rate of 120 Hz. As seen in the middle and lower panels of Fig. 8, the end-effector, whether angled or not, repeats almost the same course three times. Oscillations at the end of the measured trajectory were detectable. These oscillations arise because of the inertial force generated by the movement of the driving unit and a decrease in stiffness in the  $x$ - $y$  plane when the robot length increases. The fact that the robot has not reached the end of the trajectory slightly is probably due to model errors and joint friction. The root mean square errors (RMSE) of the average of the three experiments were approximately 17.2 mm and 2.6 degrees for the case of not angled, respectively, and 18.6 mm and 6.7 degrees for the case of angled, respectively.

### E. Demonstration

In this section, we present three demonstrations which help the intuitive understanding of the advantages of the proposed mechanism: (i) folding mechanism, (ii) follow-the-leader (FTL) deployment, and (iii) manipulation test.

Fig. 9 shows a snapshot of the manipulator during deployment and storage. The manipulator goes forward and back smoothly along with the guide for to fold with a diameter of 140 mm. It took 10 s to extend 220 mm, and then 10 s to retract. The backbone behind the driving unit, which is fixed to the base, is more flexible than the rest and thus can be stored in a small space. This is because the manipulator stiffness depends on how the proximal ends of the rack gears are connected. For example, the tension of the rack gear with the fixed proximal end changes depending on external loads. In contrast, the tension of the rack gear with the free end becomes zero, which makes the manipulator have higher compliance.

Fig. 10 shows a snapshot of the manipulator during FTL deployment, which refers to the deployment of the entire tool body, not just its tip, on a selected trajectory. The body sections can follow the track traced by the end-effector. This capability would be helpful for conducting inspections because it can be safely deployed to hard-to-reach targets while avoiding (or minimizing contact with) critical structures. A narrow pass with a length of 280 mm, a width of 90 mm, and two arcs ( $\phi 85$  mm and  $\phi 90$  mm) was set as the target trajectory. The manipulator reached the end of the pass in 13.4 s without collision.

Fig. 11 shows snapshots of whole-arm grasping. Grasping a heavy object in the horizontal plane twists a continuum robot, reducing its ability to manipulate the object and thus requiring a design with high torsional strength [27], [28]. To demonstrate our robot's high stiffness and dexterity, we prepared three objects with weights between 220g and 300g and diameters between 25mm and 100mm. The manipulator wrapped around all objects by increasing the arm length and then successfully lifted them by reducing the length. The 220g weight could be lifted almost horizontally, but the manipulator twisted slightly when lifting the 300g weight, which arise because of the backlash of the joints. The proposed mechanism can adapt its shape to objects with different diameters because the length of the first and second sections can be changed significantly by moving the driving unit.

## IV. CONCLUSIONS

We designed and constructed a woodpecker's tongue-inspired robot arm to overcome the low stiffness of existing robot arms capable of extending and bending. Our extendable and bendable mechanism based on a chain of rigid joints with flexible rack gears can selectively increase the gravitational and torsional stiffness of the robot arm. In our prototype, even simple joints with screws and bushings showed 4.7 and 6.2 times higher stiffness in gravity and torsion directions than an equivalent arm with no joints, respectively. The stiffness could be significantly increased using joints with rotary shafts and bearings, although the robot size would increase slightly as a result. Another advantage of rigid links is that the



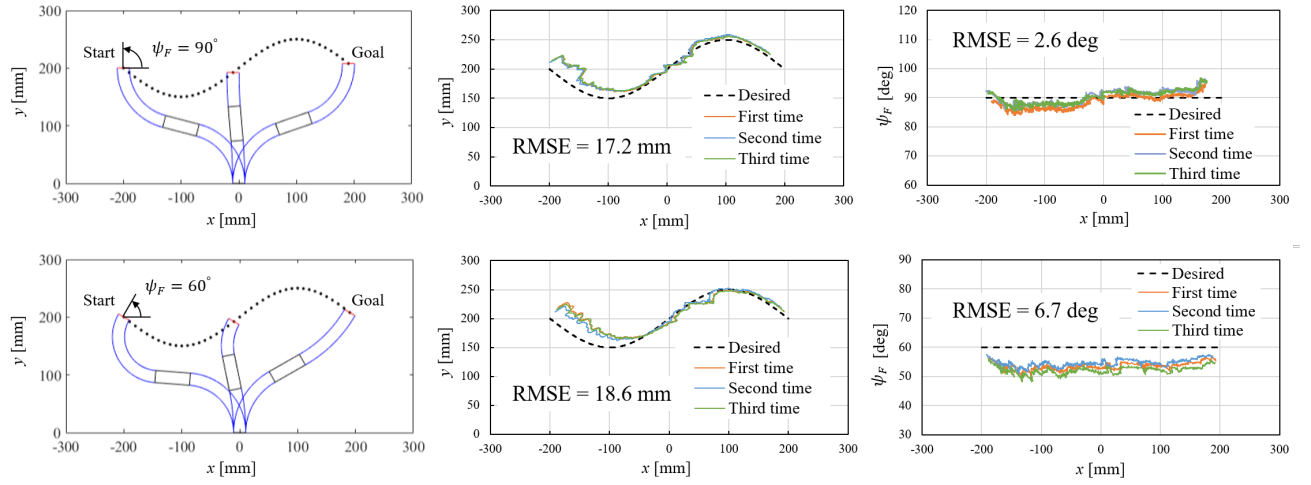


Fig. 8: Trajectory tracking test of the end-effector. The robot followed a sine curve with the tip straight as shown in the upper figures or tilted as shown in the lower figures. The left figures show the robot shape predicted by the model. The middle and right graphs show the coordinates and angle of the robot tip, respectively. The root mean squared errors (RMSE) are taking the average of three trials.

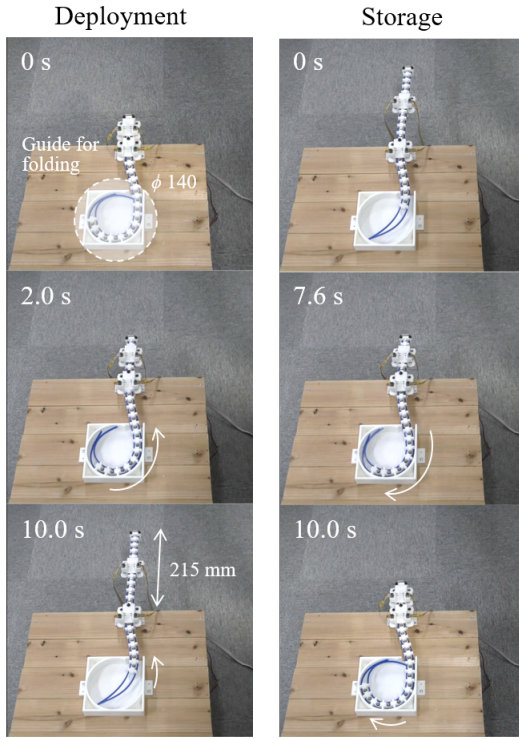


Fig. 9: Deployment and storage of the manipulator body along the guide for folding.

sliders on either side constrain the deformation of the flexible racks, providing a wide bending angle for the robot. In our experiments, we confirmed that the robot can bend along an arc up to approximately 120 degrees. An extensible body based on a rack and pinion mechanism can also increase reachability of the robot end-effector compared to an extensible mechanism based on an elastic backbone and wire-driven. A summary of

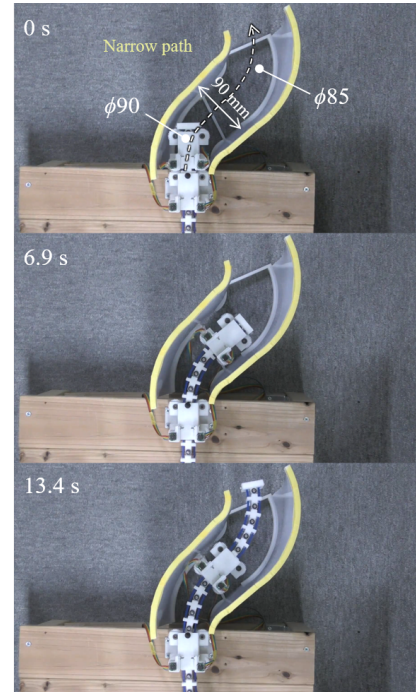


Fig. 10: Deployment of the entire robot body on a selected trajectory.

our research is presented in the Supplementary Video.

Moreover, we developed a geometric model of the manipulator for motion planning. Experiments demonstrated that the end-effector could track the desired coordinates and orientation, although it vibrated somewhat due to the inertia caused by the movement of the driving unit. The manipulator with four motors has a redundant DoF and thus has arbitrary constraints for motion control. In future work, we will investigate the

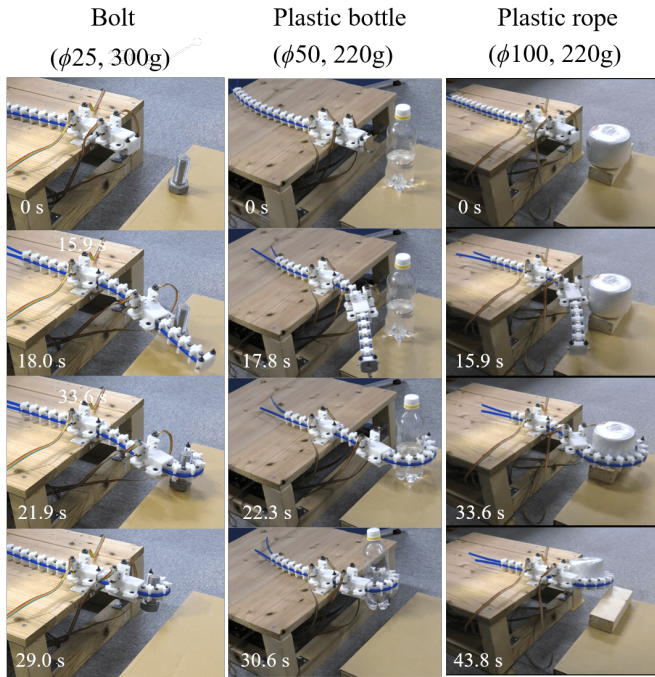


Fig. 11: Whole-arm grasping for three objects with different diameters.

manipulator's behavior under various cost functions by evaluating, for example, the stiffness ellipse of the end-effector and the inertia of the driving unit.

There are opportunities for further research and development. For example, the use of universal joints instead of revolute joints would allow the manipulators to move in three-dimensional space, and for the backbone to be folded compactly in a helical shape. Perhaps unsurprisingly, the gravitational stiffness was lower in this system than in the conventional system. However, our robot can still support a higher payload than most continuum robots because it can exert a larger force via its rigid links.

## REFERENCES

- [1] A. C. Noel and D. L. Hu, "The tongue as a gripper," *Journal of Experimental Biology*, vol. 221, no. 7, p. jeb176289, 2018.
- [2] S. Raimi, *Spider-Man 2 [Motion Picture]*. Columbia Pictures, 2004.
- [3] P. K. Singh and C. M. Krishna, "Continuum arm robotic manipulator: A review," *Universal Journal of Mechanical Engineering*, vol. 2, no. 6, pp. 193–198, 2014.
- [4] T. da Veiga, J. H. Chandler, P. Lloyd, G. Pittiglio, N. J. Wilkinson, A. K. Hoshier, R. A. Harris, and P. Valdastrì, "Challenges of continuum robots in clinical context: A review," *Progress in Biomedical Engineering*, vol. 2, no. 3, p. 032003, 2020.
- [5] S. Kim, C. Laschi, and B. Trimmer, "Soft robotics: a bioinspired evolution in robotics," *Trends in biotechnology*, vol. 31, no. 5, pp. 287–294, 2013.
- [6] J. Burgner-Kahrs, D. C. Rucker, and H. Choset, "Continuum robots for medical applications: A survey," *IEEE Transactions on Robotics*, vol. 31, no. 6, pp. 1261–1280, 2015.
- [7] D. Trivedi, C. D. Rahn, W. M. Kier, and I. D. Walker, "Soft robotics: Biological inspiration, state of the art, and future research," *Applied bionics and biomechanics*, vol. 5, no. 3, pp. 99–117, 2008.
- [8] G. Immega and K. Antonelli, "The ksi tentacle manipulator," in *Proceedings of 1995 IEEE international conference on robotics and automation*, vol. 3. IEEE, 1995, pp. 3149–3154.
- [9] K. Zhang, C. Qiu, and J. S. Dai, "An extensible continuum robot with integrated origami parallel modules," *Journal of Mechanisms and Robotics*, vol. 8, no. 3, p. 031010, 2016.
- [10] T.-D. Nguyen and J. Burgner-Kahrs, "A tendon-driven continuum robot with extensible sections," in *2015 IEEE/RSJ International Conference on Intelligent Robots and Systems (IROS)*. IEEE, 2015, pp. 2130–2135.
- [11] H. Jiang, Z. Wang, X. Liu, X. Chen, Y. Jin, X. You, and X. Chen, "A two-level approach for solving the inverse kinematics of an extensible soft arm considering viscoelastic behavior," in *2017 IEEE International Conference on Robotics and Automation (ICRA)*. IEEE, 2017, pp. 6127–6133.
- [12] H.-S. Yoon and B.-J. Yi, "A 4-dof flexible continuum robot using a spring backbone," in *Proc. IEEE Int. Conf. Mech. and Automation (ICMA)*, 2009, pp. 1249–1254.
- [13] E. W. Hawkes, L. H. Blumenschein, J. D. Greer, and A. M. Okamura, "A soft robot that navigates its environment through growth," *Science Robotics*, vol. 2, no. 8, 2017.
- [14] K. Hosaka, H. Tsukagoshi, and A. Kitagawa, "Mobile robot by a drawing-out type actuator for smooth locomotion inside narrow and curving pipes," in *Proc. 8th JFPS Int. Symp. Fluid Power*, 2011, p. 6.
- [15] T. Takahashi, M. Watanabe, K. Tadokuma, M. Konyo, and S. Tadokoro, "Retraction mechanism of soft torus robot with a hydrostatic skeleton," *IEEE Robotics and Automation Letters*, vol. 5, no. 4, pp. 6900–6907, 2020.
- [16] J.-w. Suh, K.-y. Kim, J.-w. Jeong, and J.-j. Lee, "Design considerations for a hyper-redundant pulleyless rolling joint with elastic fixtures," *IEEE/ASME Transactions on Mechatronics*, vol. 20, no. 6, pp. 2841–2852, 2015.
- [17] A. Yeshmukhametov, K. Koganezawa, and Y. Yamamoto, "A novel discrete wire-driven continuum robot arm with passive sliding disc: Design, kinematics and passive tension control," *Robotics*, vol. 8, no. 3, p. 51, 2019.
- [18] S. Teshigawara and H. H. Asada, "A mobile extendable robot arm: singularity analysis and design," in *2019 IEEE/RSJ International Conference on Intelligent Robots and Systems (IROS)*. IEEE, 2019, pp. 5131–5138.
- [19] "Hello robot," <https://hello-robot.com/>, online; visited 26-June-2021.
- [20] J. Li, R. Liu, L. Zhang, S. Zuo, and H. Wang, "Configuration synthesis and design of a telescopic service robot," in *2018 International Conference on Virtual Reality and Intelligent Systems (ICVRIS)*. IEEE, 2018, pp. 442–445.
- [21] H. Matsuo, H. H. Asada, and Y. Takeda, "Design of a novel multiple-dof extendable arm with rigid components inspired by a deployable origami structure," *IEEE Robotics and Automation Letters*, vol. 5, no. 2, pp. 2730–2737, 2020.
- [22] W. J. Bock, "Functional and evolutionary morphology of woodpeckers," *Ostrich*, vol. 70, no. 1, pp. 23–31, 1999.
- [23] J.-Y. Jung, S. E. Naleway, N. A. Yaraghi, S. Herrera, V. R. Sherman, E. A. Bushong, M. H. Ellisman, D. Kisailus, and J. McKittrick, "Structural analysis of the tongue and hyoid apparatus in a woodpecker," *Acta biomaterialia*, vol. 37, pp. 1–13, 2016.
- [24] A. Kanada and T. Mashimo, "Mobile continuum robot with unlimited extensible sections," in *2018 IEEE/RSJ International Conference on Intelligent Robots and Systems (IROS)*. IEEE, 2018, pp. 7117–7122.
- [25] A. Kanada, F. Giardina, T. Howison, T. Mashimo, and F. Iida, "Reachability improvement of a climbing robot based on large deformations induced by tri-tube soft actuators," *Soft robotics*, vol. 6, no. 4, pp. 483–494, 2019.
- [26] P. Rao, Q. Peyron, S. Lilge, and J. Burgner-Kahrs, "How to model tendon-driven continuum robots and benchmark modelling performance," *Frontiers in Robotics and AI*, vol. 7, p. 223, 2021.
- [27] J. Santoso, E. H. Skorina, M. Luo, R. Yan, and C. D. Onal, "Design and analysis of an origami continuum manipulation module with torsional strength," in *2017 IEEE/RSJ International Conference on Intelligent Robots and Systems (IROS)*. IEEE, 2017, pp. 2098–2104.
- [28] W. McMahan, V. Chitrakaran, M. Csencsits, D. Dawson, I. D. Walker, B. A. Jones, M. Pritts, D. Dienno, M. Grissom, and C. D. Rahn, "Field trials and testing of the octarm continuum manipulator," in *Proceedings 2006 IEEE International Conference on Robotics and Automation, 2006. ICRA 2006*. IEEE, 2006, pp. 2336–2341.